ELSEVIER

Journal of Alloys and Compounds 388 (2005) 308–313

Journal of ALLOYS AND COMPOUNDS

www.elsevier.com/locate/jallcom

Microstructural characterization of sol–gel derived $Pb_{1-x}La_xTiO_3$ ferroelectrics

Jun Chen, Xianran Xing*, Ranbo Yu, Jinxia Deng, Guirong Liu

Department of Physical Chemistry, University of Science and Technology Beijing, Xueyuan Road 30, Beijing 100083, China

Received 9 July 2004; received in revised form 30 July 2004; accepted 30 July 2004

Abstract

The ferroelectrics $Pb_{1-x}La_xTiO_3$ with good stoichiometry were prepared by a sol–gel route in the composition range from $x = 0.0$ up to 0.4 in 0.05 increment. The compounds were indexed in a tetragonal phase for $0.0 \leq x < 0.25$, and in a cubic phase for $0.25 \leq x < 0.4$. A tiny amount of pyrochlore phase $La_2Ti_2O_7$ was detected at $x = 0.4$. The ion oxidation states of solid solution compounds were characterized by X-ray photoelectric spectroscopy (XPS) and electron spin resonance (ESR). For the compounds $Pb_{1-x}La_xTiO_3$ prepared in the atmosphere, the electrical neutrality is kept not by the reduction from Ti^{4+} to Ti^{3+}, but by the creation of cation vacancies in the A- and B-sites. The grain size of $Pb_{1-x}La_xTiO_3$ increases with increasing La content.

Keywords: $Pb_{1-x}La_xTiO_3$; X-ray powder diffraction; XPS; SEM; Valence fluctuations

1. Introduction

Lanthanum doped lead titanate ceramics have emerged as highly promising materials for piezo-mechanical and pyroelectric applications due to their large electro-mechanical anisotropy in the coupling factors along and perpendicular to the direction of polarization and due to the large pyroelectric coefficient along the polarization axis [1,2]. These modified materials can be applied in optical waveguides, infrared sensors, dynamic random access memories and non-volatile memories [3]. In general, these properties of lanthanum doped lead titanate materials mostly depend on the lanthanum concentration. One of the characteristics can be optimized by adjusting the molar ratio of Pb/La. For example, the solid solution compound $Pb_{0.9}La_{0.1}TiO_3$ (PLT10) shows a prominent pyroelectric effect [2,4], whereas $Pb_{0.72}La_{0.28}TiO_3$ (PLT28) possesses a strong electro-optic effect [5].

In the system of solid solution $Pb_{1-x}La_xTiO_3$ (PLT), a reduction of Ti^{4+} to Ti^{3+} or some vacancies in the cation sites must be produced in order to maintain electrical neutrality. In the fabrication process, several methods were employed to maintain electrical neutrality. For example, this kind of compounds can be prepared by creating cation vacancies in A-sites or in B-sites [6–8], or can be synthesized under a reducing atmosphere reducing Ti^{4+} ions to Ti^{3+} [9]. The properties of PLT are influenced not only by the vacancy concentration but also by the Ti^{3+} concentration to a certain extent. The local structural defects introduced by B-site vacancies have much more inhibiting effects on the macroscopic cubic-to-tetragonal transition than the A-site vacancies, and the magnitude of net polarization in the PLT-B is smaller than in the PLT-A [6,7]. It is well known that the electrical neutrality could be compensated in both the A-site and the B-site, and the effects of the vacancies on the ferroelectric properties have been widely investigated. However, it has hardly been investigated whether the electrical neutrality can be partially compensated by the reduction of Ti^{4+} to Ti^{3+} in PLT compounds prepared in the atmosphere. To better understand the maintenance of electrical neutrality in the PLT system, the stoichiometry has to be taken into account. However, it is difficult to accurately control the stoichiometry because of lead oxide volatilization at high temperature in the solid-state reaction process or in some film fabrication

* Corresponding author. Tel.: +86 10 62334200; fax: +86 10 62333477.
E-mail address: xing@ustb.edu.cn (X. Xing).

0925-8388/$ – see front matter © 2004 Elsevier B.V. All rights reserved.
doi:10.1016/j.jallcom.2004.07.038

process such as magnetron sputtering, metalorganic chemical vapor deposition (MOCVD), etc [10]. The sol–gel method was adopted due to its outstanding character of controlling the stoichiometry and due to a lower sintering temperature [11].

In the present work, the solid solution compounds PLT were synthesized by a sol–gel method. The solubility limit was investigated by X-ray diffraction (XRD) at room temperature. The valence of titanium was characterized by X-ray photoelectron spectroscopy (XPS) and electron spin resonance (ESR). The micrographs of sintered ceramics PLT were characterized by scanning electron microscope (SEM).

2. Experimental procedures

Samples of $Pb_{1-x}La_xTiO_3$ were prepared by a sol–gel route, where x varied from 0.0 to 0.4 in 0.05 increments. Precursor materials were lead (II) acetate [$Pb(OCOCH_3)_2{\cdot}3H_2O$], lanthanum (III) nitrate [$La(NO_3)_3{\cdot}6H_2O$] and tetrabutyl titanate [$Ti(OC_4H_9)_4$]. Both methyl alcohol (CH_3OH) and ethylene glycol monoethyl ether [$HO(CH_2)_2OC_2H_5$] were used as solvents. Glacial acetic acid (CH_3COOH) was used as catalyst. The synthesis processes have been described in detail elsewhere [11,12].

Phase identification and structural characterization were carried out by a 21 kW extra-power powder XRD (Model M21XVHF22, Mac Science, Yokohama, Japan) at room temperature with Cu Kα radiation, and pure silicon powder was added to the sample as an internal standard. The lattice parameters were calculated by the softwares PowderX and TREOR. The DSC and TG measurements (Model STA 409, Netzsch Geraetebau, Germany) were carried in air at a heating rate of 10 °min^{-1} with α-Al_2O_3 powder as a reference. Cross sections of the ceramic samples were examined with SEM (Model LEO 1530, LEO Electron Microscopy Ltd., Germany). The average size of the grains was determined by the linear intercept method. Ion oxidation states in the samples were analyzed by X-ray photoelectron spectroscopy (Model Phi-5300 ESCA, Philadelphia, USA) with Al Kα radiation. The vacuum of the analysis chamber was maintained below 2.9×10^{-7} Pa. ESR measurements were carried out in an automated radio spectrometer (Model ER D-SRC, Bruker, Germany) in the X- and Q-region at room temperature.

3. Results and discussion

The DSC and TGA measurements of the xerogel $Pb_{09}La_{0.1}TiO_3$ (PLT10) are shown in Fig. 1. The first endothermic peak with a weight loss of about 3.07% at 80 °C corresponds to the evaporation of the water and alcohol. The next two exothermic peaks (235.2 °C) and (309.9 °C) with a weight loss of about 22.3% are caused by the decomposition of the butoxide groups and the stabilizing agent in the xerogel.

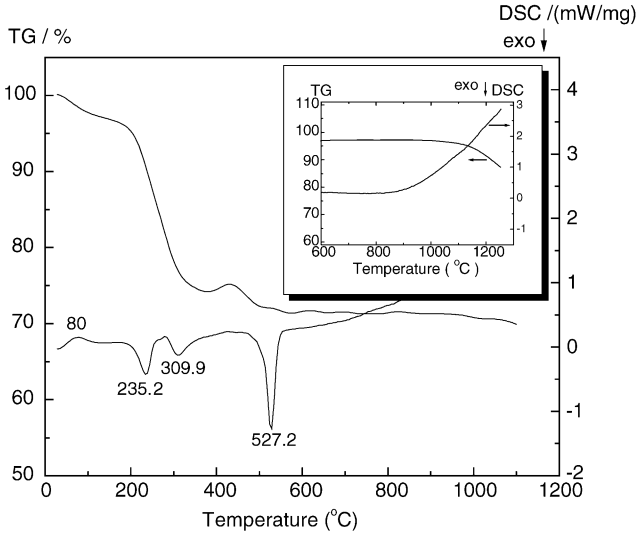

Fig. 1. DSC and TG curves of $Pb_{0.9}La_{0.1}TiO_3$ gel as function of temperature and with inset curves of the $Pb_{0.7}La_{0.3}TiO_3$ calcined at 800 °C for 2 h.

The last exothermic peak (527.2 °C) is attributed to the formation of polycrystalline PLT10, which is also confirmed by XRD measurement (see Fig. 2(a)). When the powders were calcined at 550 °C, the perovskite phase was formed without any impurity phase. Above 1050 °C, the light weight loss is due to lead oxide evaporation. For the compound PLT30 calcined at 800 °C, the weight loss occurs obviously above 1050 °C (see inset of Fig. 1). Therefore, the calcining temperature of the xerogel was carried out at 950 °C for 2 h in the present work so that the evaporation of PbO could be controlled.

The crystallization development of PLT10 is shown in Fig. 2. The peak separation between the 0 0 1 and 1 0 0 reflections and the tetragonality (c/a) increase with the calcining temperature. When the sample was calcined at a lower temperature, 550 °C, the compound was crystallized incom-

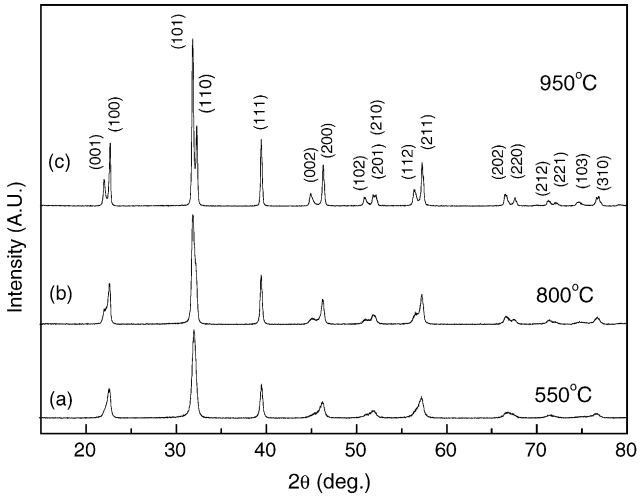

Fig. 2. XRD patterns of the $Pb_{0.9}La_{0.1}TiO_3$ solid solution with the calcining temperature: (a) 550 °C; (b) 800 °C; (c) 950 °C.

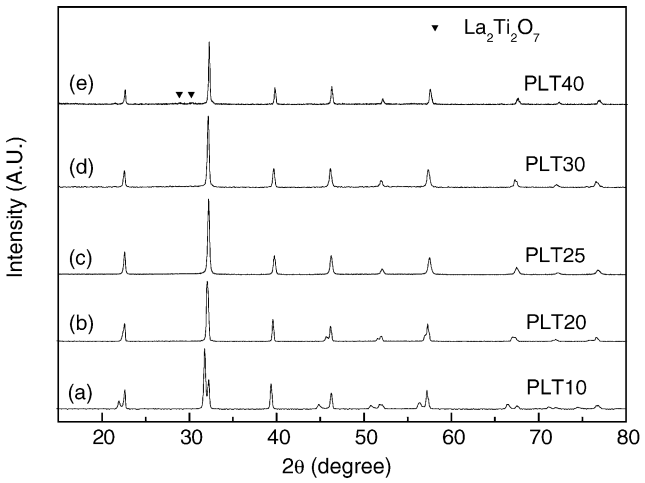

Fig. 3. XRD patterns of the $Pb_{1-x}La_xTiO_3$ solid solution with the solubility x (calcined at 950 °C for 2 h): (a) $x = 0.10$; (b) $x = 0.20$; (c) $x = 0.25$; (d) $x = 0.30$; (e) $x = 0.40$.

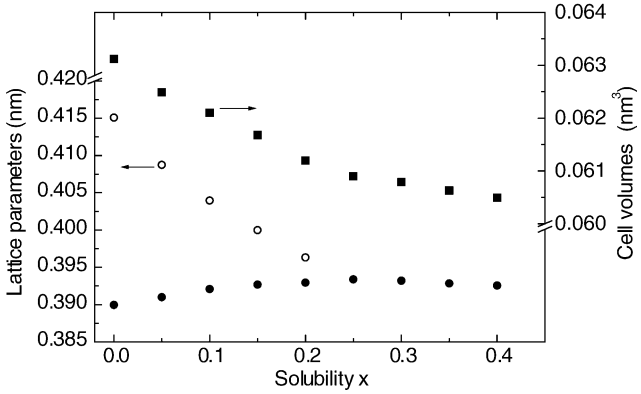

Fig. 4. Lattice parameters and cell volumes of the $Pb_{1-x}La_xTiO_3$ solid solution for solubilities of $x = 0.0$ to 0.40. (◯) c-axis, (●) a, b-axis, (■) cell volume.

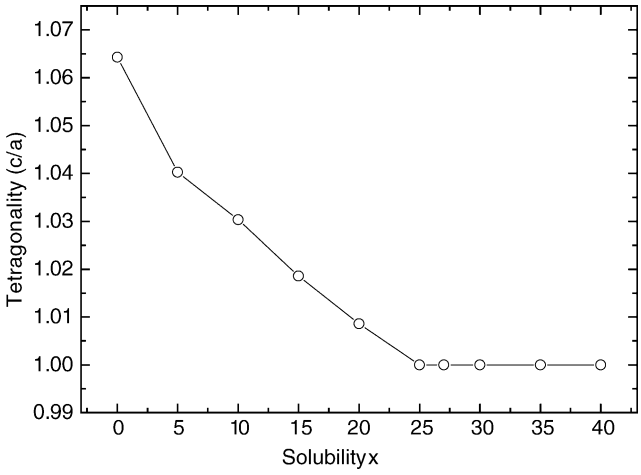

Fig. 5. The tetragonality (c/a) of $Pb_{1-x}La_xTiO_3$ in the solubility range of $0.0 \leq x \leq 0.40$.

pletely. The tetragonal structure of PLT10 can be developed fully at a calcining temperature of 950 °C (see Fig. 2(c)). No differences could be detected from the XRD patterns of the PLT compound calcined at a higher temperature. For the PLT compound calcined at different temperatures, both the Curie temperature and the tetragonality of the poorly crystallized grains become lower than those of the completely crystallized grains [12].

Fig. 3 shows that single phase PLT can be formed for $0.0 \leq x < 0.4$, and a small amount of $La_2Ti_2O_7$ pyrochlore phase was detected in the XRD patterns for $x = 0.4$. The solid solution compound PLT was indexed in a tetragonal structure for $0.0 \leq x \leq 0.20$, and in a cubic one for $0.25 \leq x < 0.40$ (see Fig. 4). It was found that the a-axis increases slightly, while the c-axis and the cell volume decrease dramatically for $0.0 \leq x \leq 0.20$. Both the lattice parameters and the cell volumes decrease for $0.25 \leq x < 0.40$. The structural parameters of PLT are listed in Table 1. Furthermore, the tetragonality (c/a) decreases almost linearly with La content in the tetragonal phase (see Fig. 5), suggesting that the tetragonal–cubic transition temperature (T_c) decreases with increasing La concentration. The result obtained for the lattice parameters of PLT in the present work is in good agreement with those of PLT-A and PLT-B which were prepared by a solid state reaction method by Kim et al. [6,7] which indicates that the lattice parameters reflect intrinsic microcrystalline characteristics of these compounds, rather than being related to the defect type and the processing parameters such as chemical homogeneity.

Micrographs of $Pb_{1-x}La_xTiO_3$ ($x = 0.10, 0.15, 0.20, 0.30$) were obtained by SEM (see Fig. 6). As shown in Table 1, the average grain size of PLT increases with the La content. Because the decrease in the tetragonality reduces the anisotropy among the grains and the stress at the grain boundaries, the grains can grow more easily with decreasing stress at the grain boundaries. The average grain size of PLT compounds depends mostly on the tetragonality. Moreover, the average

Table 1
Microstructure parameters of $Pb_{1-x}La_xTiO_3$

Composition	Tetragonal phase					Cubic phase		
	0.00	0.05	0.10	0.15	0.20	0.25	0.30	0.35
a (b)	3.8975 (6)	3.9160 (6)	3.9208 (2)	3.9269 (3)	3.9295 (2)	3.9328 (7)	3.9320 (3)	3.9285 (1)
c	4.1482 (5)	4.0738 (5)	4.0397 (1)	3.9999 (3)	3.9632 (5)	3.9328 (7)	3.9320 (3)	3.9285 (2)
c/a	1.064 (3)	1.040 (3)	1.030 (3)	1.018 (5)	1.008 (5)	1.0	1.0	1.0
Grain size (μm)			0.26	0.39	0.47		0.48	

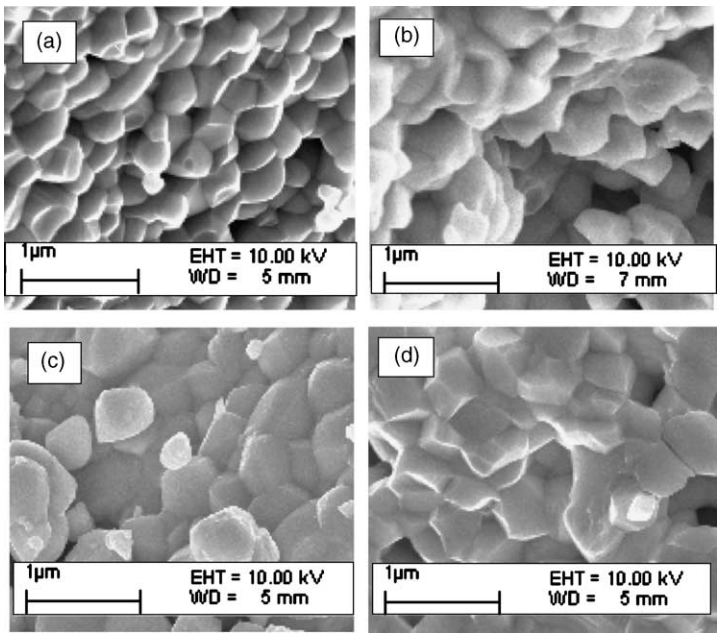

Fig. 6. SEM micrographs of the $Pb_{1-x}La_xTiO_3$ compounds: (a) PLT10; (b) PLT15; (c) PLT20; (d) PLT30.

grain size (0.26–0.48 μm) of PLT derived from a sol–gel route is much smaller than that (1–3 μm) obtained by a solid-state reaction, as reported by Tickoo et al. [13]. The grain refinement can improve the mechanical and dielectric properties.

For the PLT compounds prepared in air, it is possible that the positive charge of lanthanum becomes partly compensated by the reduction of Ti^{4+} ions. However, such assumption is not supported by experimental results in the present work. Fig. 7 shows the XPS survey spectrum of PLT20. It can be seen that the compound PLT20 contains Pb, La, Ti, O and C. A quantitative analysis of XPS data using Pb 4f, La 3d, Ti 2p and O 1s peaks revealed a A/B/O atomic ratio of 1:1:3, indicating a good stoichiometry of the compound. For the PLT20, the measured binding energies of 458.23 eV for the Ti $2p_{3/2}$ peak, 138.1 eV for the Pb $4f_{7/2}$ peak and 529.23 eV

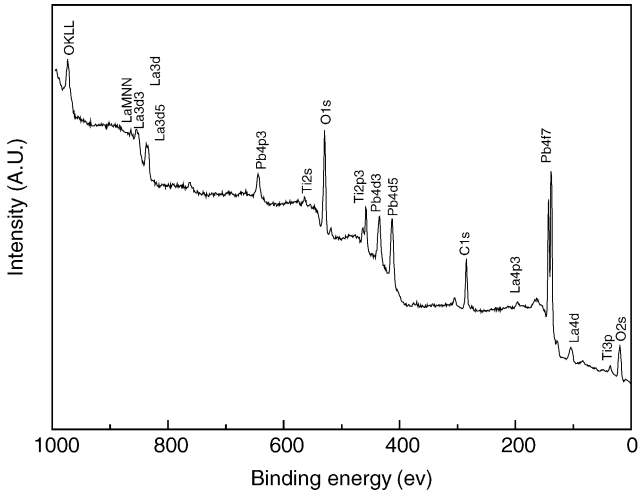

Fig. 7. XPS spectrum of $Pb_{0.8}La_{0.2}TiO_3$ calcined at 950 °C for 2 h.

for the O 1s peak are in agreement with reported data [10,14]. In the case of Ti 2p of PLT20 (see Fig. 8(a)), the two components were fitted for Ti $2p_{1/2}$ at 463.85 eV and Ti $2p_{3/2}$ at 458.23 eV, which indicates that Ti^{4+} cation is coordinated with six O^{2-} anions such as $PbTiO_3$.

The physical basis of the chemical shift effect can be explained by the following charge potential model suggested by Siegbahn et al. [15]

$$E_b^i = kq_i + \sum_j \frac{q_j}{r_{ij}} + E_b^{ref} \quad (1)$$

where E_b^i is the particular electron binding energy on atom i, q_i the charge on atom i, k a constant related to atomic radius, q_j the charge on atom j which neighbors atom i, r_{ij} the distance between atom i and atom j and E_b^{ref} the electron binding energy for reference. In the PLT system, the binding energy of Ti^{4+} is larger than that of Ti^{3+}, because both Ti^{4+} and Ti^{3+} form bonds with the same neighbor environment of oxygen atoms. If the Ti^{3+} cation exists in the compound PLT20, both the Ti $2p_{3/2}$ and the Ti $2p_{1/2}$ peaks would split into two components, respectively, which corresponds to the different valence of Ti^{4+} and Ti^{3+}. With the shape of the Ti 2p peak and the fitting result, the conclusion can be drawn that only small amounts of Ti^{3+} exist in the compounds PLT obtained by the sol–gel method. Furthermore, this conclusion can be confirmed by ESR measurements. In the samples of PLT10 and PLT20, the Ti^{3+} spectrum (g = 1.93) [16] could not be detected. Consequently, the positive charge of La_A could be compensated by vacancies in the A- and B-sites without reduction of Ti^{4+}. Fig. 8 also demonstrates that each peak shifts toward higher binding energies of approximate 0.2–0.5 eV with increasing La content. The increase in bind-

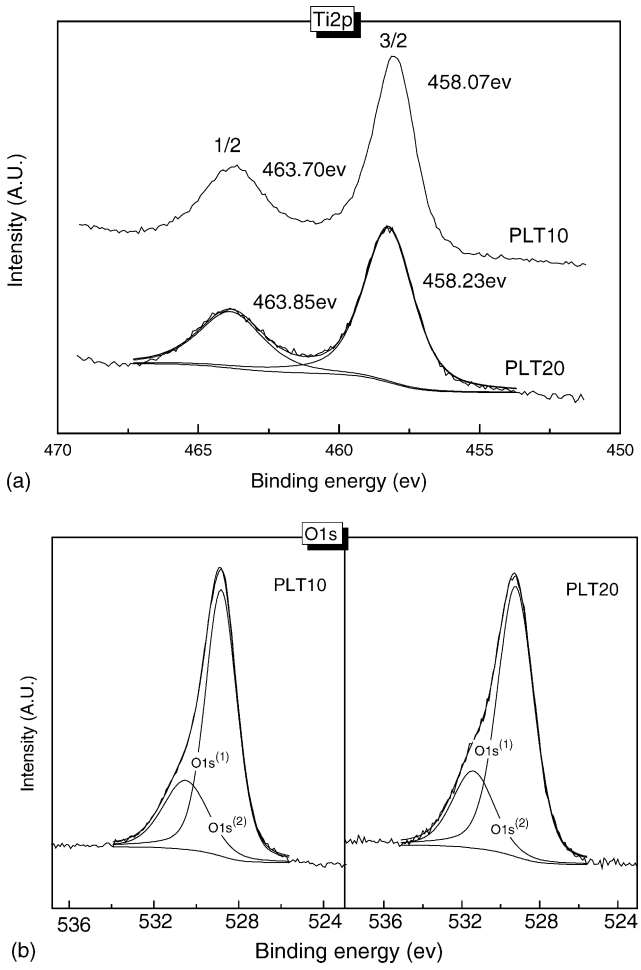

Fig. 8. (a) Ti 2p and (b) O 1s XPS spectra of $Pb_{0.9}La_{0.1}TiO_3$ and $Pb_{0.8}La_{0.2}TiO_3$ with peak fitting.

ing energies of Ti 2p arises from the decrease in r_{ij}, and that of O 1s from the increase in q_j and the decrease in r_{ij} with increasing solubility x. In the O 1s spectra shown in Fig. 8 (b), the curve fitting was performed by a Gaussian function and a good fit to the peak shape was obtained. The O 1s peak is composed of the O 1s $^{(1)}$ peak and the O 1s $^{(2)}$ peak. The O 1s $^{(1)}$ peak energy corresponds to the oxygen in the PLT lattice, including Pb–O, La–O and Ti–O bonding, and the O 1s $^{(2)}$ peak is due to absorbed oxygen on the surface such as hydroxyl groups. If oxygen vacancies exist in the PLT compounds, the O 1s $^{(2)}$ peak can also be composed of oxygen vacancies [15]. The ratio of the area under the O 1s $^{(2)}$ and O 1s $^{(1)}$ peaks will increase with increasing oxygen vacancy concentration. The ratios of PLT10 and PLT20 are 36.9% and 34.8% respectively, which indicates that the ratio of the area almost remains constant with increasing La content in the present investigation. This behavior might result from some PbO volatilization, and the oxygen vacancy concentration is depressed in a low level, which is consistent with the TGA results in Fig. 1. Therefore, the electrical neutrality is retained by the creation of cation vacancies in the A- and B-sites, not by the reduction from Ti^{4+} to Ti^{3+}.

In the lanthanum doped lead titanate system, the composition of the homogenous perovskite phase can be described by the following formula [8]:

$$Pb_{3(1-ax)/3+x(1.5-a)}La_{3x/3+x(1.5-a)}\square_{x(2a-1.5)/3+x(1.5-a)}[Ti_{3/3+x(1.5-a)}\square_{x(1.5-a)/3+x(1.5-a)}]O_3 \quad (2)$$

where x is the La content, and α is the lead elimination factor, which varies from 0.75 to 1.5. When PLT has A-site vacancies only, the corresponding α value is 1.5. On the other hand, if it is only characterized by the B-site vacancies, α becomes 0.75. For the present PLT system, the lead elimination α is 1.0, and it can be ascribed by the following formula.

$$Pb_{3(1-x)/3+0.5x}La_{3x/3+0.5x}\square_{0.5x/3+0.5x}[Ti_{3/3+0.5x}\square_{0.5x/3+0.5x}]O_3 \quad (3)$$

The A- and B-site vacancy concentrations increase with increasing La content, which will reduce the structural stability of the PLT compounds. Moreover, the temperature for PbO evaporation from PLT decreases with increasing La concentration [17]. When the solubility x exceeded the solubility limit of PLT, a tiny amount of $La_2Ti_2O_7$ phase was detected at $x = 0.4$ (see Fig. 3(e)).

4. Conclusions

1. $Pb_{1-x}La_xTiO_3$ compounds with good stoichiometry were prepared by a sol–gel route in the composition range of $0.0 \leq x \leq 0.4$. These compounds were indexed in the tetragonal phase for $0.0 \leq x < 0.25$, and in the cubic phase for $0.25 \leq x < 0.4$. The phase transition from the tetragonal system to the cubic one occurs at $x = 0.25$. When the La content exceeds the solubility limit ($x = 0.40$), a tiny amount of $La_2Ti_2O_7$ pyrochlore phase was detected.
2. The result of lattice parameters of PLT in the present work agrees with those of PLT-A and PLT-B, which indicates that the lattice parameters are hardly influenced by the substitution type.
3. The XPS and ESR results demonstrate that only small amounts Ti^{3+} exist in the compounds $Pb_{1-x}La_xTiO_3$. The electrical neutrality is retained not by the reduction of Ti^{4+} to Ti^{3+}, but by the creation of cation vacancies in the A- and B-sites. The concentration of the cation vacancies increases with increasing La content until the pyrochlore phase $La_2Ti_2O_7$ appears.
4. The grain size increases nonlinearly with increasing La content.

Acknowledgements

This work was supported by National Natural Science Foundation of China (No. 20331030, 50374009), and Funds

of Ministry of Education of China for TRAPOYT Program, and training Ph.D. Candidates (No. 2001008005).

References

[1] Q.C. Zhao, Y. Liu, W.S. Shi, W. Ren, L.Y. Zhang, X. Yao, Appl. Phys. Lett. 69 (1996) 458.
[2] K. Ijima, R. Takayama, Y. Tomita, I. Ueda, J. Appl. Phys. 60 (1986) 2914.
[3] W.L. Zhong, Ferroelectric Physics, Science Press, Beijing, 2000.
[4] S. Chen, M.D. Liu, C.R. Li, Y.K. Zeng, J.D. Costa, Thin Solid Films 375 (2000) 188.
[5] S. Bhaskar, S.B. Majumder, M. Jain, P.S. Dobal, P.S. Katiyar, Mater. Sci. Eng. B 87 (2001) 178.
[6] T.Y. Kim, H.M. Jang, S.M. Cho, J. Appl. Phys. 91 (2002) 336.
[7] T.Y. Kim, H.M. Jang, Appl. Phys. Lett. 77 (2000) 3824.
[8] D. Hennings, Mater. Res. Bull. 6 (1971) 329.
[9] R. Moos, K.H. Härdtl, J. Appl. Phys. 80 (1996) 393.
[10] H.Y. Chen, J. Lin, K.L. Tan, Z.C. Feng, Thin Solid Films 289 (1996) 59.
[11] G.A. Rossetti Jr., L.E. Cross, J.P. Cline, J. Mater. Sci. 30 (1995) 24.
[12] Q.F. Zhou, H.L.W. Chan, Q.Q. Zhang, C.L. Choy, J. Appl. Phys. 89 (2001) 8121.
[13] R. Tickoo, R.P. Tandon, N.C. Mehra, P.N. Kotru, Mater. Sci. Eng. B 94 (2002) 1.
[14] Q. Zhou, H. Ruda, B.G. Yacobi, M. Farrell, Thin Solid Films 402 (2002) 65.
[15] K. Siegbahn, C. Nordling, A. Fahlman, R. Nordbeng, K. Hamrin, J. Hedman, G. Johansson, T. Bergmark, S.E. Karlsson, I. Lindgren, B. Lindberg, Nova Acta Regiae Soc. Sci. Ups. 4 (1967) 20.
[16] I.P. Bykov, M.D. Glinchuk, V.V. Laguta, Y.L. Maximenko, L. Jastrabik, V.A. Trepakov, V. Dimza, M. Hrabovsky, J. Chem. Solids 56 (1995) 919.
[17] Y. Deng, Z. Yin, Q. Chen, M.S. Zhang, W.F. Zhang, Mater. Sci. Eng. B 84 (2001) 248.